

Crossway Diffusion: Improving Diffusion-based Visuomotor Policy via Self-supervised Learning

Xiang Li Varun Belagali Jinghuan Shang Michael S. Ryoo

Department of Computer Science
Stony Brook University
{xiangli8, vbelagali, jishang, mryoo}@cs.stonybrook.edu

Abstract: Sequence modeling approaches have shown promising results in robot imitation learning. Recently, diffusion models have been adopted for behavioral cloning, benefiting from their exceptional capabilities in modeling complex data distribution. In this work, we propose Crossway Diffusion, a method to enhance diffusion-based visuomotor policy learning by using an extra self-supervised learning (SSL) objective. The standard diffusion-based policy generates action sequences from random noise conditioned on visual observations and other low-dimensional states. We further extend this by introducing a new decoder that reconstructs raw image pixels (and other state information) from the intermediate representations of the reverse diffusion process, and train the model jointly using the SSL loss. Our experiments demonstrate the effectiveness of Crossway Diffusion in various simulated and real-world robot tasks, confirming its advantages over the standard diffusion-based policy. We demonstrate that such self-supervised reconstruction enables better representation for policy learning, especially when the demonstrations have different proficiencies.

Keywords: Diffusion model, Behavioral Cloning, Self-supervised Learning

1 Introduction

Behavioral Cloning (BC) [1] is a supervised learning formulation for robot action policy learning. Given expert demonstration data consist of a sequence of state-action pairs, we train a model to predict the correct action vector given input states (e.g., images). This framework has shown to be very effective particularly when a sufficient amount of training data is provided [2].

Recently, sequence modeling approaches [3–5] have been often used for behavioral cloning, because of their ability to model multiple steps of information. In such a formulation, the objective is to model the probability distribution of the multi-step state-action trajectory. This allows BC to consider beyond a single-step regression, better taking advantage of history. Given the success in modeling human language [6] and images [7], Transformers [8] have been popularly adopted for the sequence modeling-based policies [3, 4, 2].

Diffusion models [9, 10], an approach to model data distribution, also have been applied for sequential modeling recently [11, 12]. Diffusion models have exceptional capabilities in modeling multimodal data distribution and generating new samples from the distribution, which make them suitable for imitating behaviors by generating trajectories. For visuomotor control tasks, Chi et al. [13] demonstrated promising performance on real-world tasks with high-dimensional multimodal controls, using visual observations as conditions of the diffusion model.

In this work, we propose Crossway Diffusion, a simple yet effective method to improve diffusion-based visuomotor policy learning using an extra self-supervised learning (SSL) objective. Specifically, we introduce an SSL task that reconstructs the raw pixels and other state information from

the intermediate representations of the reverse diffusion (denoising) process. This reconstruction task forces the model to focus on both the observation and action features. It also encourages the temporal correspondence between the latent representations.

Through our experiments over multiple challenging tasks from different benchmarks, we verify the consistent advantage of Crossway Diffusion in various simulated and real-world robot tasks in comparison to the baseline Diffusion Policy. Especially, we achieve a $\sim 15\%$ improvement over the baseline on Transport, mh dataset from Robomimic [14], as well as in our real robot evaluation. Our contribution can be summarized as follow:

- We propose Crossway Diffusion, a simple yet effective way to improve diffusion-based vasomotor policy learning using a self-supervised auxiliary loss during training. Compare to the baseline, Crossway Diffusion requires no additional computation during evaluation.
- We confirm the effectiveness of the proposed method on multiple challenging visual BC tasks from different benchmarks and collect our real-world robot manipulation dataset.
- We conduct detailed ablations on multiple design choices of Crossway Diffusion as well as one contrastive learning-based auxiliary loss. We observe that two variants of Crossway Diffusion also bring consistent improvement over the baseline, indicating the robustness of our proposed method.

2 Preliminaries

Behavioral Cloning We consider simple behavioral cloning (BC) setting over a Markov Decision Process (MDP), described by the tuple $(\mathcal{S}, \mathcal{A}, P)$, where $s \in \mathcal{S}$ represents the state, $a \in \mathcal{A}$ is the action, and P are the transition dynamics given by $P(s'|s, a)$. A trajectory consists of a sequence of state-action pairs $\{s_0, a_0, s_1, a_1, \dots, s_T, a_T\}$. Our goal is to train a robot policy π that best recovers an unknown policy π^* using a demonstration dataset $\mathcal{D} = \{(s_i, a_i)\}$ collected by π^* . Specifically, the robot policy π operates on a trajectory basis: $\pi(A_t|S_t)$, where $S_t = \{s_{t-T_s+1}, s_{t-T_s+2}, \dots, s_t\}$ is the given short history state sequence, $A_t = \{a_t, a_{t+1}, \dots, a_{t+T_a-1}\}$ is the predicted future actions to take. T_s and T_a represent the lengths of these two sequences respectively.

Diffusion Models Diffusion models [15, 10] are generative models that iteratively generate samples that match the data distribution. The diffusion process is of the original data being destroyed by a sequence of noise $q(x^k|x^{k-1})$ known as the forward process, where k is the current diffusion step and there are K steps in total. The diffusion model uses the reverse process, the backward process, $p_\theta(x^{k-1}|x^k)$ to denoise the corrupted data. By iteratively denoising, a diffusion model generates synthesized data \hat{x} that approximates the original data distribution $q(x_0)$, starting from a random prior $p(x^K)$:

$$p_\theta(x^0) := \int p_\theta(x^{0:K}) dx^{1:K} = \int p(x^K) \prod_{k=1}^K p_\theta(x^{k-1}|x^k) dx^{1:K} \quad (1)$$

Typically the random prior $p(x^K)$ is a standard Gaussian distribution, and the denoising process is parameterized by the following Gaussian:

$$p_\theta(x^{k-1}|x^k) = \mathcal{N}(x^{k-1}|\mu_\theta(x^k, k), \Sigma^k), \quad (2)$$

where the parameter $\mu_\theta(x^k, k)$ is estimated from the model, usually implemented as a neural network parameterized by θ .

Diffusion-based Policy Diffusion models [16–18, 10, 19] have demonstrated the great ability in image generation and other data generation tasks. Recent works in robotics [3–5, 20–22, 11] formulate the robot policy learning as an action sequence generation problem, taking advantage of sequence modeling methods like Transformer and diffusion model. Janner et al. [11] concatenate the low-dimensional system states and the action at each time step as a vector and models multiple state-action pairs as a matrix (image) generation problem. However, such a configuration is not

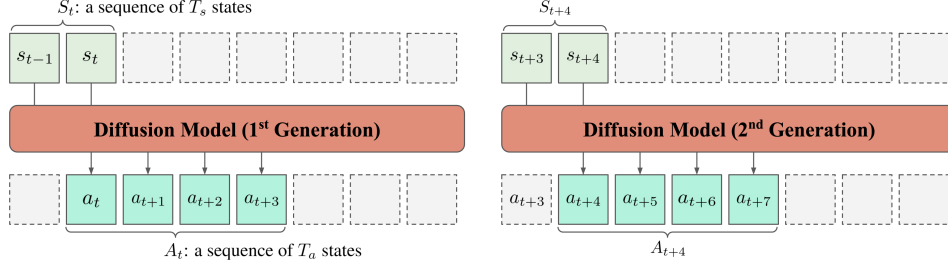


Figure 1: Trajectory generation formulation of Diffusion Policy

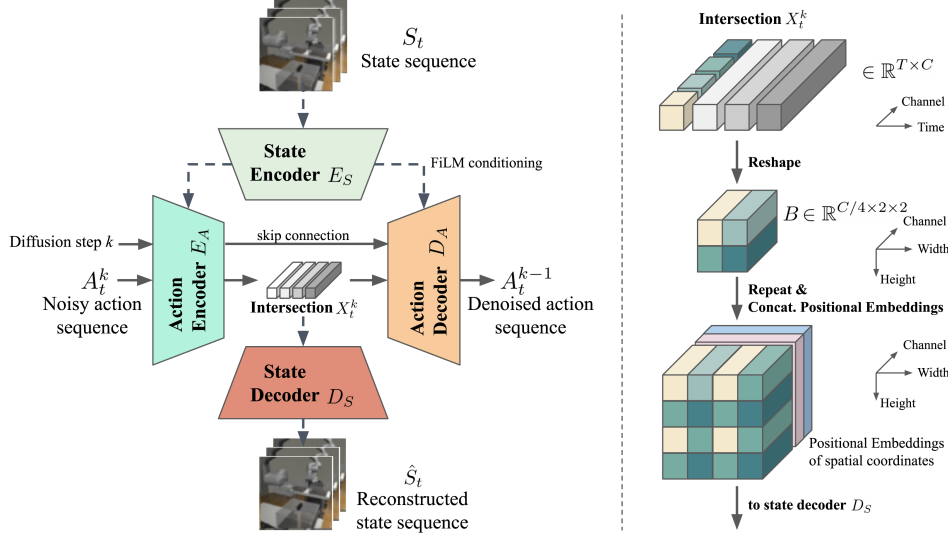


Figure 2: Left: Architecture of Crossway Diffusion. Crossway Diffusion introduces a state decoder head to the existing Diffusion Policy [13] architecture. The state decoder takes a transformed intermediate action embedding ‘intersection’ to reconstruct the original input state. Right: Transformation applied to ‘intersection’ before applying the state decoder.

feasible for visuomotor policy learning due to the high dimensionality of the visual observations. Diffusion Policy [13] tackles the challenge by generating only action sequences using DDPM [9], while the generation process is under the condition of visual observations.

3 Method

Crossway Diffusion extends Diffusion Policy [13] by introducing (1) a state decoder for state reconstruction and (2) an auxiliary reconstruction loss to be jointly optimized with the diffusion loss during training. We follow the standard problem formulation that treats behavioral cloning as an action sequence generation problem conditioned on states. Specifically, given a sequence of T_s states $S_t = \{s_{t-T_s+1}, s_{t-T_s+2}, \dots, s_t\}$ which contains both visual states and low-dimensional states, the diffusion model (action encoder and decoder) generates a sequence of T_a actions $A_t = \{a_t, a_{t+1}, \dots, a_{t+T_a-1}\}$ (see Figure 1). Note that the actual sequence length T_p generated by the diffusion model is usually larger than T_a , due to padding. After the agent finishes executing A_t , the diffusion model will generate the consequent action sequence given the current state sequence S_{t+T_a} , which formulates a closed-loop control.

Architectural Overview The overall architecture of Crossway Diffusion is presented as Figure 2. We introduce a new state decoder module D_S for state reconstruction, extending the existing Diffusion Policy model composed of a state encoder E_S , an action encoder E_A , and an action decoder D_A . The action encoder and decoder make up the diffusion model for generating action se-

quences by running the diffusion process iteratively. The state encoder provides conditioning from the states, which modulates the generation process.

For any state sequence S_t , the state encoder, which is a modified ResNet18 [23] introduced by [13], extracts a batch of visual embeddings $h_{t,img}$ from every single image in S_t . The visual embeddings are then concatenated with other low dimensional states $S_{t,low-dim}$ to format the observation condition. The process above is described as Equation 3:

$$\begin{aligned} S_t &= \{S_{t,img}, S_{t,low-dim}\} \\ h_{t,img} &= E_S(S_{t,img}) \\ h_t &= h_{t,img} \oplus S_{t,low-dim} \end{aligned} \quad (3)$$

The action encoder E_A and decoder D_A are made of 1D conditional residual CNN blocks and down/upsampling modules similar to a UNet [24] in DDPM [9]. The action encoder E_A takes the noisy action sequence A_t^k at diffusion step k and the observation condition h_t and produces the representation X_t^k from the deepest layer and other tensors for skip connection $X_{t,skip}^k$ from the shallower layers:

$$X_t^k, X_{t,skip}^k = E_A(A_t^k, h_t, k) \quad (4)$$

where t is the timestamp of a state or action trajectory (See Figure 1). $X_t^k \in \mathbb{R}^{T \times C}$ where T is the representation length along the time axis and C is the number of channels.

The action decoder takes both $X_t^k, X_{t,skip}^k$ and condition h_t to estimate the noise applied to A_t^k in the forward diffusion process. The condition h_t is applied between two convolutional layers in the residual block, using Feature-wise Linear Modulation (FiLM) [25]. Then we derive a (slightly) denoised action sequence A_t^{k-1} from the estimated noise ϵ_θ and A_t^k using Equation 5.

$$\begin{aligned} \epsilon_\theta &= D_A(X_t^k, X_{t,skip}^k, h_t) \\ A_t^{k-1} &= \frac{1}{\sqrt{\alpha_k}} \left(A_t^k - \frac{1 - \alpha_k}{\sqrt{1 - \alpha_k}} \epsilon_\theta \right) + \sigma_k z \end{aligned} \quad (5)$$

where z is randomly sampled from a normal distribution and it has the same dimension as A_t^k . $\alpha_k, \hat{\alpha}_k$ and σ_k are parameters regarding the diffusion process used in the original DDPM [9] paper, except that we use k instead of t as the diffusion step. During inference, the denoising process mentioned above is repeated for K times iteratively, generating a noiseless action sequence A_t^0 in the end through the repeated application of the action encoder and decoder. A_t^0 is the action sequence our method generates for robot control as shown in Figure 1.

The state decoder D_S reconstructs the input states from a transformed intermediate representation $\hat{S}_t = D_S(g(X_t^k))$, where \hat{S}_t is the reconstructed states and $g(\cdot)$ is the *intersection transformation*, which we will discuss more in the following subsection and Section 4.3.

The representation X_t^k is dubbed *intersection* since both the flow of action sequence denoising and the flow of state sequence reconstruction pass through this tensor and then head to their corresponding destinations. For the same reason, we name our method *Crossway Diffusion*, whose key feature is to have two flows above intersected.

For each source of the state, we assign a dedicated decoder for the best reconstruction results. To reconstruct the visual states, the state decoder is made of 2D residual CNN blocks and upsampling similar to a 2D UNet decoder but without skip connections. While other low-dim states are processed by two-layer MLPs using the vanilla intersection tensor.

Notice that the reconstruction with the state decoder D_S is only used during the training, serving as an ‘interpreter’ to generate additional supervisory signals to train better intermediate representations. The reconstruction itself is not used during the inference.

Intersection Transformation for Image Reconstruction We transform the intersection tensor X_t^k before sending it to the visual state decoder, bridging the dimensional gap between the action sequence embedding and image embeddings.

As shown in the right of Figure 2, we first divide the intersection tensor X_t^k along the time axis and now it can be regarded as a list of vectors with a length of C . In the default setting of Crossway Diffusion, only the *first* vector is selected. The C elements of the first vector are equally split into 4 folds and then tiled as a $C/4 \times 2 \times 2$ block B . The tile block B is repeated multiple times in two spatial dimensions so that it will have a spatial resolution of a quarter of the desired reconstructed image along each spatial dimension. Finally, we encode the 2D pixel location (normalized to $[-1, 1]$) using the same method from NeRF [26], and the positional embedding is concatenated to the repeated B along the channel axis, which finishes the intersection transformation. The visual state decoder will reconstruct the image sequence from the concatenated tensor. We also investigate other design choices of the intersection transformation in Section 4.3.

Crossway Diffusion Loss In addition to DDPM loss \mathcal{L}_{DDPM} used in Diffusion Policy [13], the reconstruction task provides an auxiliary self-supervised loss \mathcal{L}_{Recon} , which is a Mean Squared Error (MSE) between the reconstructed states and the original input states. The reconstruction loss \mathcal{L}_{Recon} is jointly optimized along with \mathcal{L}_{DDPM} by simple addition. The total loss for Crossway Diffusion is denoted as Equation 6 where ϵ is the noise applied to A_t^0 for constructing A_t^k and we find $\alpha = 0.1$ is a generally good setting without extensive hyperparameter search.

$$\begin{aligned}\mathcal{L}_{DDPM} &= \text{MSE}(D_S(E_A(A_t^k, h_t, k), h_t), \epsilon) \\ \mathcal{L}_{Recon} &= \text{MSE}(S_t, \hat{S}_t) \\ \mathcal{L}_{Crossway} &= \mathcal{L}_{DDPM} + \alpha \mathcal{L}_{Recon}.\end{aligned}\tag{6}$$

4 Experiment

We evaluate Crossway Diffusion on four challenging simulated tasks and one real-world task from multiple benchmarks. Furthermore, we explore two variants of Crossway Diffusion regarding intersection transformation and one direct extension of Crossway Diffusion taking advantage of contrastive learning. Through a series of conducted experiments, we confirm that Crossway Diffusion leads to better performance than the vanilla Diffusion Policy baseline [13] over all the tested tasks, especially when the demonstrations are varied in proficiency. We also show that our method is robust to unseen obstructions in real-world environment settings.

4.1 Task and Dataset

We follow [13] and choose three challenging tasks Square, Transport, and Tool Hang from Robomimic [14] and Push-T from Implicit Behaviour Cloning (IBC) [27]. In addition, we build a real-world robot arm manipulation environment and collect our own data for the task Duck Lift.

In the ‘Square’ task, the robot needs to fit the square nut onto the square peg. The ‘Transport’ task entails the collaborative effort of two robot arms to transfer a hammer from a closed container situated on one table to a designated bin on another table. One arm is responsible for retrieving and passing the hammer, while the other arm manages the trash disposal and receives the passed hammer. In ‘Tool Hang’, the objective is to complete the assembling of a frame, which comprises a base piece and a hook piece. The robot needs to insert the hook into the base and then hang a wrench on the hook. Additionally, the ‘Push-T’ task involves pushing a T-shaped block (gray) onto a target location (green) in a 2D space. Regarding the expert proficiency of demonstrations, we investigate two datasets with the Transport task: ‘ph’ - proficient-human demonstration and ‘mh’ - multi-human demonstrations, defined by original Robomimic [14]. ‘mh’ is designed to have lower proficiency on the task in average compared to ‘ph’.

In the real-world task ‘Duck Lift’, the objective is to pick up a rubber duck using a robot arm with a gripper and images from two cameras. The first camera is stationary and offers a third-person perspective of the operating space, while the second camera is mounted on the gripper, providing a first-person view for grasping. The action space encompasses both the 3D position of the robot arm and a binary signal for the gripper’s opening and close.

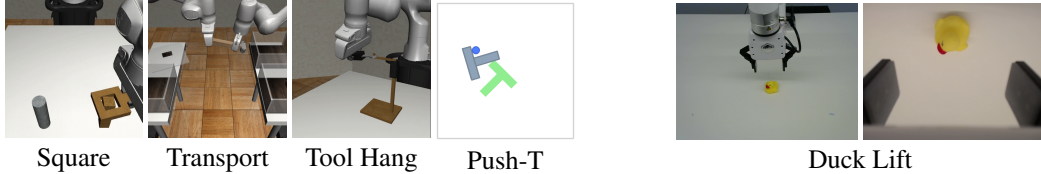


Figure 3: Left: Visual reference for simulated tasks. Right: two camera views in Duck Lift.

A visual reference for all these tasks is provided in Figure 3. Detailed information on all the datasets is summarized in Table 1.

Table 1: Dataset summary. Type: demonstration type, ph: proficient-human demonstrations, mh multi-human demonstrations; # Demos: the number of demonstrations; Real?: whether the dataset is a real-world dataset or not; # of Rob.: the number of robots; # of Obj.: the number of objects; # of Cam.: the number of cameras; Act-D: action dimension; Steps: max number of rollout steps.

Task	Type	# of Demos	Real?	# of Rob.	# of Obj.	# of Cam.	Act-D	Steps
Square	mh	300	N	1	1	2	7	400
Transport	mh	300	N	2	3	4	14	700
Transport	ph	200	N	2	3	4	14	700
Tool Hang	ph	200	N	1	2	2	7	700
Push-T	ph	200	N	1	1	1	2	300
Duck Lift	ph	100	Y	1	1	2	4	50

4.2 Main Results

Evaluation Metrics Consistent with prior studies, we adopt the success rate of the following tasks, Square, Transport, Tool Hang, and Duck Lift, as a performance metric. In the case of the Push-T task, we measure the extent of target location coverage achieved by the T block, which is the ratio of the covered area to the total area. All the models are trained for 500 epochs and evaluated at the end of training. For all diffusion-based methods, we benchmark the exponential moving average (EMA) version of the model for better stability, as suggested by [9]. More training details are available in Appendix A.1. Figure 9 shows example episodes using Crossway Diffusion for each task.

Simulated Experiments For all the simulated tasks, we report the average performance over 1000 randomly initialized episodes \times 3 models trained with different random seeds in Table 2. That is, each score in Table 2 is an average of 3000 experiments in total. From the comparison, the proposed Crossway Diffusion consistently outperforms the baseline Diffusion Policy [13] in all datasets. Especially, we observed a 15.7% improvement in *Transport, mh*, emphasizing the effectiveness of our method when the demonstration data is varied in proficiency. Please refer to Figure 9 for the example episodes generated by our method.

Real-world Experiments The results of Duck Lift are reported in Table 3. The success rate of picking up the duck is measured over 20 episodes. For each episode, we place the duck at a random initial position but keep the positions consistent across tested methods. The results show that our method achieves a higher success rate than the baseline Diffusion Policy [13]. We further

Table 2: Results on five challenging simulated datasets. We report the average performance over 1000 episodes \times 3 models trained with different random seeds.

Method	Square, mh	Transport, mh	Transport, ph	Tool Hang	Push-T
LSTM-GMM	0.491	0.254	0.656	0.474	0.567
IBC [27]	0.000	0.000	0.000	0.000	0.687
Diffusion Policy CNN [13]	0.858	0.643	0.859	0.772	0.819
Crossway Diffusion (Ours)	0.879	0.800	0.864	0.792	0.843

Table 3: Results of Duck Lift

	Diffusion Policy CNN [13]	Crossway Diffusion (Ours)
Succ.%	0.80	0.95

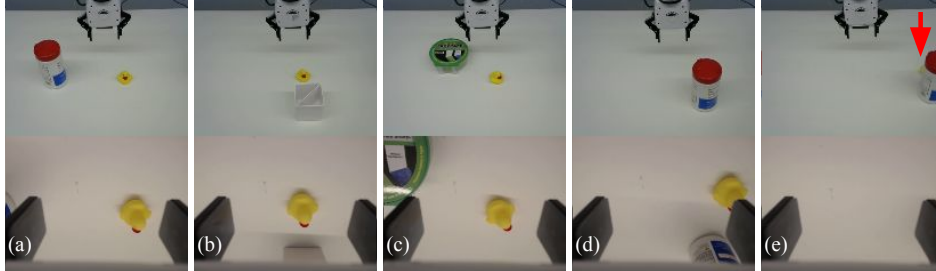


Figure 4: Duck Lift task under different obstructions (a,b,c,d,e). The first row and second row show the two camera views respectively. The red arrow in (e) is used to indicate the position of the duck.

validate the robustness of our method under various obstructions as shown in Figure 4. None of these obstructions are present in the training dataset. Figure 4 (a)(b)(c) contain different unseen objects placed on the table as a distraction. In Figure 4 (d), the duck is only visible to the second camera. Our method successfully executes the task in all the above scenarios indicating robustness to obstructions. Figure 4 (e) shows a scenario where the duck is not clearly visible to both cameras. In this case, as expected our method fails to locate and lift the duck.

Qualitative Results on Image Reconstruction In Figure 5, we show multiple pairs of original (left) and reconstructed (right) images randomly selected from the validation set. For simulated environments, Crossway Diffusion provides surprisingly well-reconstructed images given the abundance of data. For real-world environments, the reconstructions preserve most of the robot and duck structures, while failing on the details (mouth and eyes) of the duck. However, we note that bad reconstruction, especially on non-task-related details, does not necessarily mean poor performance, since the reconstruction task helps the learning process. More reconstruction examples are available in Appendix A.2.

4.3 Ablations

On Intersection Transformation We investigate two more designs of the intersection transformation displayed in Figure 6 over all five simulated datasets. Specifically, we are interested in which part of the intersection X_t^k benefits policy learning most while leaving other operations untouched. As shown in Figure 6, Design A is the default Crossway Diffusion introduced in Section 3. In Design B, the first $C/2$ channels for all vectors in intersection X_t^k are selected for reconstruction, while the rest is left dedicated to the denoising process. In contrast, Design C takes advantage of all vectors in X_t^k for the reconstruction. Additionally, the vector is independently projected by a linear layer to match the target number of channels $C/4$ in both Design B and C. The latter operations like reshape and repeat in Figure 2 are kept the same. The results presented in Table 4 show that all the design variants of intersection transformation consistently outperform the baseline Diffusion Policy. Such observations validate the effectiveness and robustness of introducing the auxiliary reconstruction objective. Though different designs show diverse advantages over different tasks, we choose Design A as the default due to its computational simplicity.

On Auxiliary SSL Task In default Crossway Diffusion, both images and low-dimensional states are reconstructed from the intersection. We first benchmark a simple variant of Crossway Diffusion called *Crossway-Visual* on Push-T, which reconstructs only the image states rather than all the states.

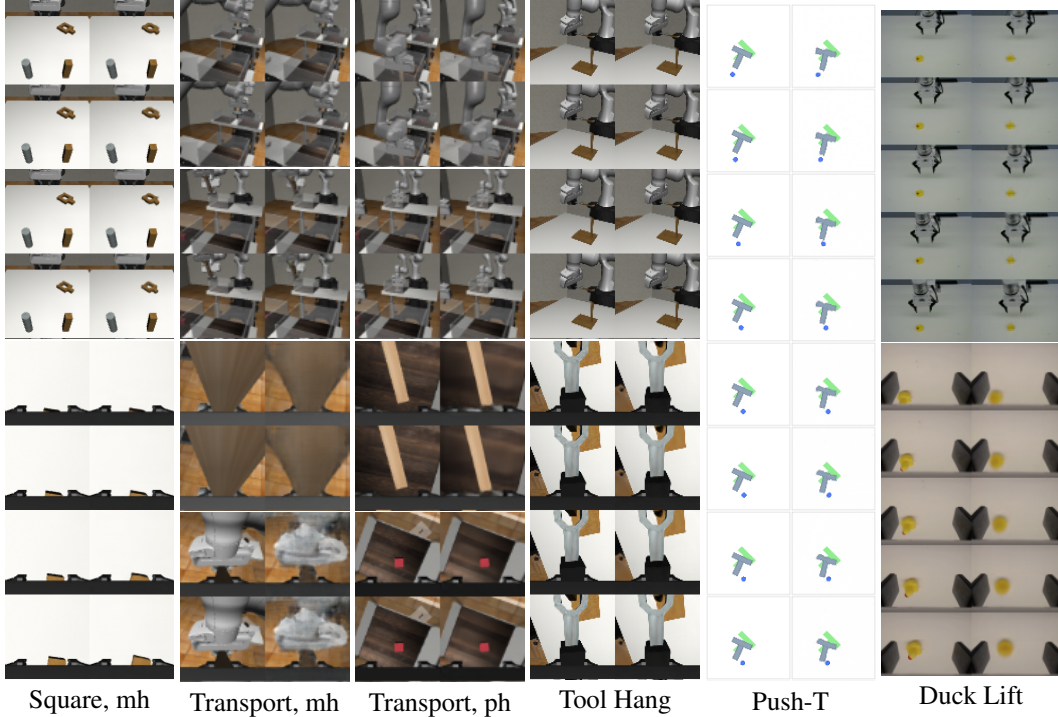


Figure 5: Image reconstruction results on the validation set. For each dataset, left: original image, right: reconstructed image. More examples are available in Appendix A.2.

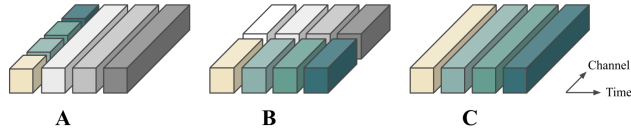


Figure 6: Three different designs of our ‘intersection’ transformation for the ablation study.

Furthermore, we verify the effectiveness of the reconstruction auxiliary task, in comparison to another self-supervised learning approach using contrastive learning inspired by CURL [28]. In particular, we independently perform random crop on all images of an observation sequence S_t twice to get two augmented sequences $S_{t,a1}$ and $S_{t,a2}$. The model takes $S_{t,a1}$ to produce intersection $X_{t,a1}^k$ while $S_{t,a2}$ is processed by the exponential moving average (EMA) version of the model to get $X_{t,a2,ema}^k$. The intuition is that due to the semantic similarity between $S_{t,a1}$ and $S_{t,a2}$, the intersection $X_{t,a1}$ and $X_{t,a2,ema}$ should also be similar in a latent space. We follow CURL [28] and maintain a learnable matrix W . For each batch of samples, we calculate the similarity matrix M_{sim} between all samples in the same batch using matrix multiplication (first line in Equation 7). Then the contrastive loss \mathcal{L}_{CURL} is formulated as maximizing the similarity between the same sample while minimizing the similarity between different samples, which is equivalent to a cross-entropy loss. Finally the contrastive loss \mathcal{L}_{CURL} is jointly optimized with the diffusion loss \mathcal{L}_{DDPM} similar

Table 4: Ablation results on the intersection transformation design. We use the same metric as Table 2. All Crossway Diffusion variants consistently outperform the baseline.

Method	Square, mh	Transport, mh	Transport, ph	Tool Hang	Push-T
Ours - Design A (default)	0.879	0.800	0.864	0.792	0.843
Ours - Design B	0.881	0.784	0.882	0.777	0.835
Ours - Design C	0.868	0.814	0.906	0.783	0.831
Diffusion Policy CNN [13]	0.858	0.643	0.859	0.772	0.819

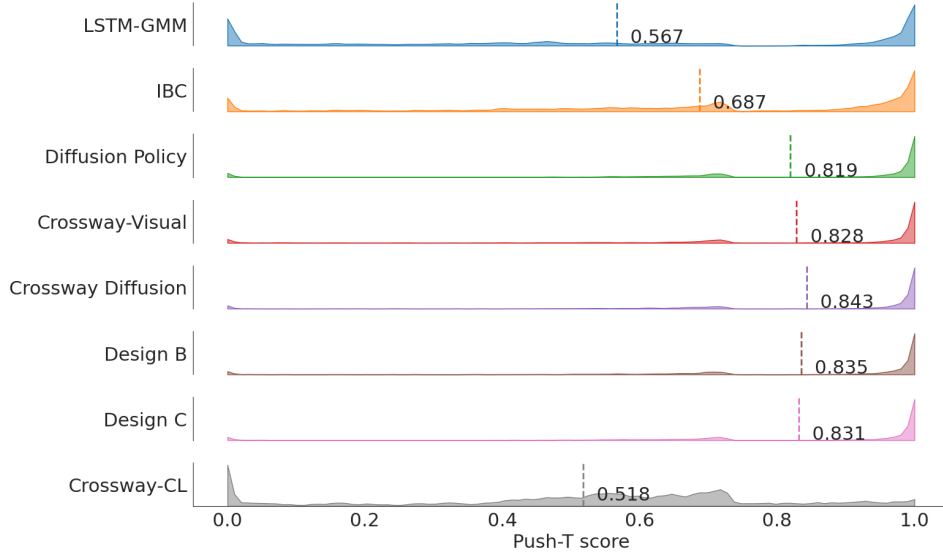


Figure 7: Push-T score distributions using the same metric as Table 2. The mean score is noted as the dashed line. Reconstructing only visual observations (Crossway-Visual) will slightly compromise the performance compared to reconstructing all states. While contrastive learning loss (Crossway-CL) significantly decreases performance.

to Equation 6. The loss computation is presented as Equation 7, where $\text{sg}(\cdot)$ means stop gradients, b is the batch size and we set $\alpha = 0.1$ same as the default setting. We name such configuration as *Crossway-CL*.

$$\begin{aligned}
 M_{\text{sim}} &= X_{t,a1}^k \cdot W \cdot \text{sg}(X_{t,a2,\text{ema}}^k)^T \\
 \mathcal{L}_{\text{CURL}} &= \text{CrossEntropyLoss}(M_{\text{sim}}, \text{range}(b)) \\
 \mathcal{L}_{\text{Crossway-CL}} &= \mathcal{L}_{\text{DDPM}} + \alpha \mathcal{L}_{\text{CURL}}
 \end{aligned} \tag{7}$$

The results are shown in Figure 7. From Figure 7, we observe that the variant which only reconstructs visual observations (Crossway-Visual) achieves performance that lies between Crossway Diffusion and the baseline. This finding confirms the significance of reconstructing both images and low-dimensional states. The contrastive learning variant Crossway-CL yields much worse performance compared to the baseline, indicating that not all self-supervised auxiliary losses benefit policy learning. Such observations happen to align with the online reinforcement learning case [29].

5 Related Work

Behavioral Cloning Behavioral Cloning (BC) [1, 30, 31] is a straightforward but surprisingly effective way to obtain robot policies due to its simplicity compared to RL. With pre-collected state-action pairs, BC learns a policy like fitting a dataset [32], with additional techniques like reward labeling / IRL [33, 34], distribution matching [35, 36], and incorporating extra information [37–39]. Apart from explicitly generating output actions, BC can be done implicitly, where an energy-based model is learned to model the action distribution [27]. Implicit BC is found to be effective in real-world robot tasks. BC also boosts some online RL algorithms like TD3+BC [40], DeepMimic [41], and more [42]. Recent Diffusion-model based BC is more like an advanced approach for matching the behavior distribution, which potentially helps mitigate the distribution shift problem in BC [43].

Sequential Modeling for Offline-RL and Imitation Learning Sequential modeling [3, 4] is the recent direction to solve offline-RL or Imitation Learning problems. The key is to optimize a policy on a trajectory basis from pre-collected experiences, with a reward signal (offline-RL) or without it (imitation learning). To model the trajectory composed by state-action-reward tuples, Transformer [8] is firstly adopted to this problem in the light of success in modeling natural language.

In this formulation, state-action-reward tuples are regarded as equal units [3, 4] or with Markovian properties [5, 44] for better long-term modeling. There are works to extend the formulation to on-line learning [45], hindsight matching [46], and bootstrapping [47]. Recently, Diffusion-based models [10] are also adopted to this problem [11, 20] and showing promising results on robot tasks [13], and on combining with RL objectives [21, 22]. Orthogonal to robot policy learning, diffusion models can be also applied to data augmentation and synthesis for scaling [48, 49], or to robot planning using text-conditioned video generation model [50].

Self-supervised learning Self-supervised learning (SSL) [51] is used to learn data representations without task labels. SSL is commonly used to (pre-)train task-agnostic foundation models [52–54], or is used as an auxiliary task together with other learning paradigms. Similarly, SSL has multiple ways to combine with policy learning, and we briefly categorize them into two: pre-training with SSL [55–62], and policy learning jointly with auxiliary SSL tasks [63–68, 28, 69–77, 29]. Studies [29] have shown that different ways to combine policy learning with SSL have different outcomes. In this work, we follow the joint learning style that optimizes diffusion and reconstruction objectives together.

6 Limitation

Even though our self-supervised learning objective improves the performance, it remains the same need for a large number of diffusion iterations during inference as the baseline Diffusion Policy [13]. This is still a common challenge for diffusion-based policies that hinders responsiveness in some high-dynamic real-world environments. To this end, we use DDIM [10] to accelerate the inference process as suggested in [13].

7 Conclusion

In this paper, we investigate how SSL can be used to improve diffusion-based visual behavioral cloning. We propose Crossway Diffusion, which involves an extra reconstruction auxiliary objective in addition to the existing diffusion objective during training. Compare to the baseline, Crossway Diffusion requires no additional computation during evaluation and shows consistent improvements over multiple challenging tasks including one real-world task. Especially, we observe a significant performance boost when the demonstrations are varied in proficiency. We hope our work inspires further exploration of diffusion-based policies and how to take advantage of the rapidly evolving SSL techniques.

References

- [1] D. A. Pomerleau. *Alvinn: An autonomous land vehicle in a neural network*. In *NIPS*, 1988.
- [2] A. Brohan, N. Brown, J. Carbajal, Y. Chebotar, J. Dabis, C. Finn, K. Gopalakrishnan, K. Hausman, A. Herzog, J. Hsu, J. Ibarz, B. Ichter, A. Irpan, T. Jackson, S. Jesmonth, N. J. Joshi, R. Julian, D. Kalashnikov, Y. Kuang, I. Leal, K.-H. Lee, S. Levine, Y. Lu, U. Malla, D. Manjunath, I. Mordatch, O. Nachum, C. Parada, J. Peralta, E. Perez, K. Pertsch, J. Quiambao, K. Rao, M. Ryoo, G. Salazar, P. Sanketi, K. Sayed, J. Singh, S. Sontakke, A. Stone, C. Tan, H. Tran, V. Vanhoucke, S. Vega, Q. Vuong, F. Xia, T. Xiao, P. Xu, S. Xu, T. Yu, and B. Zitkovich. *Rt-1: Robotics transformer for real-world control at scale*. *arXiv preprint arXiv:2212.06817*, 2022.
- [3] L. Chen, K. Lu, A. Rajeswaran, K. Lee, A. Grover, M. Laskin, P. Abbeel, A. Srinivas, and I. Mordatch. *Decision transformer: Reinforcement learning via sequence modeling*. *Advances in neural information processing systems*, 34:15084–15097, 2021.
- [4] M. Janner, Q. Li, and S. Levine. *Offline reinforcement learning as one big sequence modeling problem*. In *Proc. Adv. Neural Inform. Process. Syst.*, Dec. 2021.
- [5] J. Shang, X. Li, K. Kahatapitiya, Y.-C. Lee, and M. S. Ryoo. *Starformer: Transformer with state-action-reward representations for robot learning*. *IEEE Transactions on Pattern Analysis and Machine Intelligence*, pages 1–16, 2022.
- [6] J. Devlin, M.-W. Chang, K. Lee, and K. Toutanova. *Bert: Pre-training of deep bidirectional transformers for language understanding*. *arXiv preprint arXiv:1810.04805*, 2018.
- [7] A. Dosovitskiy, L. Beyer, A. Kolesnikov, D. Weissenborn, X. Zhai, T. Unterthiner, M. Dehghani, M. Minderer, G. Heigold, S. Gelly, et al. *An image is worth 16x16 words: Transformers for image recognition at scale*. In *Proceedings of the International Conference on Learning Representations (ICLR)*, 2020.
- [8] A. Vaswani, N. Shazeer, N. Parmar, J. Uszkoreit, L. Jones, A. N. Gomez, Ł. Kaiser, and I. Polosukhin. *Attention is all you need*. In *Advances in Neural Information Processing Systems (NeurIPS)*, Dec. 2017.
- [9] J. Ho, A. Jain, and P. Abbeel. *Denoising diffusion probabilistic models*. *Advances in Neural Information Processing Systems*, 33:6840–6851, 2020.
- [10] J. Song, C. Meng, and S. Ermon. *Denoising diffusion implicit models*. In *International Conference on Learning Representations*, 2021.
- [11] M. Janner, Y. Du, J. B. Tenenbaum, and S. Levine. *Planning with diffusion for flexible behavior synthesis*. *arXiv preprint arXiv:2205.09991*, 2022.
- [12] A. Ajay, Y. Du, A. Gupta, J. Tenenbaum, T. Jaakkola, and P. Agrawal. *Is conditional generative modeling all you need for decision-making?* *arXiv preprint arXiv:2211.15657*, 2022.
- [13] C. Chi, S. Feng, Y. Du, Z. Xu, E. Cousineau, B. Burchfiel, and S. Song. *Diffusion policy: Visuomotor policy learning via action diffusion*. *arXiv preprint arXiv:2303.04137*, 2023.
- [14] A. Mandlekar, D. Xu, J. Wong, S. Nasiriany, C. Wang, R. Kulkarni, L. Fei-Fei, S. Savarese, Y. Zhu, and R. Martín-Martín. *What matters in learning from offline human demonstrations for robot manipulation*. *arXiv preprint arXiv:2108.03298*, 2021.
- [15] J. Sohl-Dickstein, E. Weiss, N. Maheswaranathan, and S. Ganguli. *Deep unsupervised learning using nonequilibrium thermodynamics*. In *International Conference on Machine Learning*, pages 2256–2265. PMLR, 2015.
- [16] A. Ramesh, P. Dhariwal, A. Nichol, C. Chu, and M. Chen. *Hierarchical text-conditional image generation with clip latents*. *arXiv preprint arXiv:2204.06125*, 2022.

- [17] R. Rombach, A. Blattmann, D. Lorenz, P. Esser, and B. Ommer. High-resolution image synthesis with latent diffusion models. In *Proceedings of the IEEE/CVF Conference on Computer Vision and Pattern Recognition*, pages 10684–10695, 2022.
- [18] S. Gu, D. Chen, J. Bao, F. Wen, B. Zhang, D. Chen, L. Yuan, and B. Guo. Vector quantized diffusion model for text-to-image synthesis. In *Proceedings of the IEEE/CVF Conference on Computer Vision and Pattern Recognition*, pages 10696–10706, 2022.
- [19] R. Rombach, A. Blattmann, D. Lorenz, P. Esser, and B. Ommer. High-resolution image synthesis with latent diffusion models. In *Proceedings of the IEEE/CVF Conference on Computer Vision and Pattern Recognition (CVPR)*, pages 10684–10695, June 2022.
- [20] T. Pearce, T. Rashid, A. Kanervisto, D. Bignell, M. Sun, R. Georgescu, S. V. Macua, S. Z. Tan, I. Momennejad, K. Hofmann, et al. Imitating human behaviour with diffusion models. *arXiv preprint arXiv:2301.10677*, 2023.
- [21] H.-C. Wang, S.-F. Chen, and S.-H. Sun. Diffusion model-augmented behavioral cloning. *arXiv preprint arXiv:2302.13335*, 2023.
- [22] Z. Wang, J. J. Hunt, and M. Zhou. Diffusion policies as an expressive policy class for offline reinforcement learning. *arXiv preprint arXiv:2208.06193*, 2022.
- [23] K. He, X. Zhang, S. Ren, and J. Sun. Deep residual learning for image recognition. In *Proceedings of the IEEE conference on computer vision and pattern recognition*, pages 770–778, 2016.
- [24] O. Ronneberger, P. Fischer, and T. Brox. U-net: Convolutional networks for biomedical image segmentation. In *Medical Image Computing and Computer-Assisted Intervention—MICCAI 2015: 18th International Conference, Munich, Germany, October 5-9, 2015, Proceedings, Part III 18*, pages 234–241. Springer, 2015.
- [25] E. Perez, F. Strub, H. De Vries, V. Dumoulin, and A. Courville. Film: Visual reasoning with a general conditioning layer. In *Proceedings of the AAAI Conference on Artificial Intelligence*, volume 32, 2018.
- [26] B. Mildenhall, P. P. Srinivasan, M. Tancik, J. T. Barron, R. Ramamoorthi, and R. Ng. Nerf: Representing scenes as neural radiance fields for view synthesis. In *Proceedings of the European Conference on Computer Vision (ECCV)*, pages 405–421. Springer, 2020.
- [27] P. Florence, C. Lynch, A. Zeng, O. A. Ramirez, A. Wahid, L. Downs, A. Wong, J. Lee, I. Mordatch, and J. Tompson. Implicit behavioral cloning. In *Conference on Robot Learning*, pages 158–168. PMLR, 2022.
- [28] M. Laskin, A. Srinivas, and P. Abbeel. Curl: Contrastive unsupervised representations for reinforcement learning. In *Proceedings of the International Conference on Machine Learning (ICML)*, pages 5639–5650. PMLR, 2020.
- [29] X. Li, J. Shang, S. Das, and M. Ryoo. Does self-supervised learning really improve reinforcement learning from pixels? In *Advances in Neural Information Processing Systems*, volume 35, pages 30865–30881, 2022.
- [30] L. P. Kaelbling. *Learning in embedded systems*. MIT press, 1993.
- [31] P. Kormushev, S. Calinon, and D. G. Caldwell. Imitation learning of positional and force skills demonstrated via kinesthetic teaching and haptic input. *Advanced Robotics*, 25(5):581–603, 2011.
- [32] C. G. Atkeson and S. Schaal. Robot learning from demonstration. In *Proceedings of the International Conference on Machine Learning (ICML)*, volume 97, pages 12–20, 1997.

- [33] A. Y. Ng, S. Russell, et al. Algorithms for inverse reinforcement learning. In *Proceedings of the International Conference on Machine Learning (ICML)*, volume 1, page 2, 2000.
- [34] T. Osa, J. Pajarinen, G. Neumann, J. A. Bagnell, P. Abbeel, J. Peters, et al. An algorithmic perspective on imitation learning. *Foundations and Trends® in Robotics*, 7(1-2):1–179, 2018.
- [35] J. Ho and S. Ermon. Generative adversarial imitation learning. *CoRR*, abs/1606.03476, 2016. URL <http://arxiv.org/abs/1606.03476>.
- [36] X. B. Peng, Z. Ma, P. Abbeel, S. Levine, and A. Kanazawa. Amp: Adversarial motion priors for stylized physics-based character control. *ACM Transactions on Graphics (TOG)*, 40(4): 1–20, 2021.
- [37] P. Florence, L. Manuelli, and R. Tedrake. Self-supervised correspondence in visuomotor policy learning. *IEEE Robotics and Automation Letters*, 5(2):492–499, 2019.
- [38] T. Zhang, Z. McCarthy, O. Jow, D. Lee, X. Chen, K. Goldberg, and P. Abbeel. Deep imitation learning for complex manipulation tasks from virtual reality teleoperation. In *2018 IEEE International Conference on Robotics and Automation (ICRA)*, pages 5628–5635. IEEE, 2018.
- [39] R. Rahmatizadeh, P. Abolghasemi, L. Bölöni, and S. Levine. Vision-based multi-task manipulation for inexpensive robots using end-to-end learning from demonstration. In *2018 IEEE international conference on robotics and automation (ICRA)*, pages 3758–3765. IEEE, 2018.
- [40] S. Fujimoto and S. S. Gu. A minimalist approach to offline reinforcement learning. *Advances in neural information processing systems*, 34:20132–20145, 2021.
- [41] X. B. Peng, P. Abbeel, S. Levine, and M. Van de Panne. Deepmimic: Example-guided deep reinforcement learning of physics-based character skills. *ACM Transactions On Graphics (TOG)*, 37(4):1–14, 2018.
- [42] A. Rajeswaran, V. Kumar, A. Gupta, G. Vezzani, J. Schulman, E. Todorov, and S. Levine. Learning complex dexterous manipulation with deep reinforcement learning and demonstrations. *arXiv preprint arXiv:1709.10087*, 2017.
- [43] P. Abbeel and A. Y. Ng. Apprenticeship learning via inverse reinforcement learning. In *Proceedings of the twenty-first international conference on Machine learning*, page 1, 2004.
- [44] S. Hu, L. Shen, Y. Zhang, and D. Tao. Graph decision transformer, 2023.
- [45] Q. Zheng, A. Zhang, and A. Grover. Online decision transformer, 2022.
- [46] H. Furuta, Y. Matsuo, and S. S. Gu. Distributional decision transformer for hindsight information matching. In *Proceedings of the International Conference on Learning Representations (ICLR)*, 2022.
- [47] K. Wang, H. Zhao, X. Luo, K. Ren, W. Zhang, and D. Li. Bootstrapped transformer for offline reinforcement learning. In *Advances in Neural Information Processing Systems (NeurIPS)*, 2022.
- [48] T. Yu, T. Xiao, A. Stone, J. Tompson, A. Brohan, S. Wang, J. Singh, C. Tan, J. Peralta, B. Ichter, et al. Scaling robot learning with semantically imagined experience. *arXiv preprint arXiv:2302.11550*, 2023.
- [49] C. Lu, P. J. Ball, and J. Parker-Holder. Synthetic experience replay. *arXiv preprint arXiv:2303.06614*, 2023.
- [50] Y. Dai, M. Yang, B. Dai, H. Dai, O. Nachum, J. Tenenbaum, D. Schuurmans, and P. Abbeel. Learning universal policies via text-guided video generation. *arXiv preprint arXiv:2302.00111*, 2023.

- [51] P. Vincent, H. Larochelle, Y. Bengio, and P.-A. Manzagol. Extracting and composing robust features with denoising autoencoders. In *Proceedings of the 25th international conference on Machine learning*, pages 1096–1103, 2008.
- [52] K. He, X. Chen, S. Xie, Y. Li, P. Dollár, and R. Girshick. Masked autoencoders are scalable vision learners. *arXiv:2111.06377*, 2021.
- [53] T. Brown, B. Mann, N. Ryder, M. Subbiah, J. D. Kaplan, P. Dhariwal, A. Neelakantan, P. Shyam, G. Sastry, A. Askell, et al. Language models are few-shot learners. *Advances in Neural Information Processing Systems (NeurIPS)*, 33:1877–1901, 2020.
- [54] T. Chen, S. Kornblith, M. Norouzi, and G. Hinton. A simple framework for contrastive learning of visual representations. In *International conference on machine learning*, pages 1597–1607. PMLR, 2020.
- [55] D. Ha and J. Schmidhuber. World models. *arXiv preprint arXiv:1803.10122*, 2018.
- [56] P. Sermanet, C. Lynch, Y. Chebotar, J. Hsu, E. Jang, S. Schaal, S. Levine, and G. Brain. Time-contrastive networks: Self-supervised learning from video. In *2018 IEEE international conference on robotics and automation (ICRA)*, pages 1134–1141. IEEE, 2018.
- [57] A. Zhan, P. Zhao, L. Pinto, P. Abbeel, and M. Laskin. A framework for efficient robotic manipulation. In *Advances in Neural Information Processing Systems (NeurIPS)*, 2021.
- [58] R. Shah and V. Kumar. Rrl: Resnet as representation for reinforcement learning. In *Proceedings of the International Conference on Learning Representations (ICLR)*, 2021.
- [59] A. Stooke, K. Lee, P. Abbeel, and M. Laskin. Decoupling representation learning from reinforcement learning. In *Proceedings of the International Conference on Machine Learning (ICML)*, pages 9870–9879. PMLR, 2021.
- [60] J. Shang and M. S. Ryoo. Self-supervised disentangled representation learning for third-person imitation learning. In *IEEE/RSJ International Conference on Intelligent Robots and Systems (IROS)*, pages 214–221. IEEE, 2021.
- [61] C. Wang, X. Luo, K. Ross, and D. Li. Vrl3: A data-driven framework for visual deep reinforcement learning. *arXiv preprint arXiv:2202.10324*, 2022.
- [62] T. Xiao, I. Radosavovic, T. Darrell, and J. Malik. Masked visual pre-training for motor control. *arXiv preprint arXiv:2203.06173*, 2022.
- [63] A. v. d. Oord, Y. Li, and O. Vinyals. Representation learning with contrastive predictive coding. *arXiv preprint arXiv:1807.03748*, 2018.
- [64] M. Igl, L. Zintgraf, T. A. Le, F. Wood, and S. Whiteson. Deep variational reinforcement learning for pomdps. In *Proceedings of the International Conference on Machine Learning (ICML)*, pages 2117–2126. PMLR, 2018.
- [65] D. Hafner, T. Lillicrap, I. Fischer, R. Villegas, D. Ha, H. Lee, and J. Davidson. Learning latent dynamics for planning from pixels. In *Proceedings of the International Conference on Machine Learning (ICML)*, pages 2555–2565. PMLR, 2019.
- [66] P. Yingjun and H. Xinwen. Learning representations in reinforcement learning: An information bottleneck approach. *arXiv preprint arXiv:1911.05695*, 2019.
- [67] D. Yarats, A. Zhang, I. Kostrikov, B. Amos, J. Pineau, and R. Fergus. Improving sample efficiency in model-free reinforcement learning from images. In *Proceedings of the AAAI Conference on Artificial Intelligence (AAAI)*, pages 10674–10681, 2021.

- [68] A. X. Lee, A. Nagabandi, P. Abbeel, and S. Levine. Stochastic latent actor-critic: Deep reinforcement learning with a latent variable model. *Advances in Neural Information Processing Systems (NeurIPS)*, 33:741–752, 2020.
- [69] J. Zhu, Y. Xia, L. Wu, J. Deng, W. Zhou, T. Qin, and H. Li. Masked contrastive representation learning for reinforcement learning. *arXiv preprint arXiv:2010.07470*, 2020.
- [70] B. Mazouze, R. Tachet des Combes, T. L. Doan, P. Bachman, and R. D. Hjelm. Deep reinforcement and infomax learning. *Advances in Neural Information Processing Systems (NeurIPS)*, 33:3686–3698, 2020.
- [71] K.-H. Lee, I. Fischer, A. Liu, Y. Guo, H. Lee, J. Canny, and S. Guadarrama. Predictive information accelerates learning in rl. *Advances in Neural Information Processing Systems (NeurIPS)*, 33:11890–11901, 2020.
- [72] Z. D. Guo, B. A. Pires, B. Piot, J.-B. Grill, F. Altché, R. Munos, and M. G. Azar. Bootstrap latent-predictive representations for multitask reinforcement learning. In *Proceedings of the International Conference on Machine Learning (ICML)*, pages 3875–3886. PMLR, 2020.
- [73] M. Schwarzer, A. Anand, R. Goel, R. D. Hjelm, A. Courville, and P. Bachman. Data-efficient reinforcement learning with momentum predictive representations. In *Proceedings of the International Conference on Learning Representations (ICLR)*, 2021.
- [74] A. Zhang, R. McAllister, R. Calandra, Y. Gal, and S. Levine. Learning invariant representations for reinforcement learning without reconstruction. In *Proceedings of the International Conference on Learning Representations (ICLR)*, 2021.
- [75] T. Yu, C. Lan, W. Zeng, M. Feng, Z. Zhang, and Z. Chen. Playvirtual: Augmenting cycle-consistent virtual trajectories for reinforcement learning. *Advances in Neural Information Processing Systems (NeurIPS)*, 34, 2021.
- [76] T. D. Kulkarni, A. Gupta, C. Ionescu, S. Borgeaud, M. Reynolds, A. Zisserman, and V. Mnih. Unsupervised learning of object keypoints for perception and control. *Advances in Neural Information Processing Systems (NeurIPS)*, 32, 2019.
- [77] X. Wang, L. Lian, and S. X. Yu. Unsupervised visual attention and invariance for reinforcement learning. In *Proceedings of the IEEE/CVF Conference on Computer Vision and Pattern Recognition (CVPR)*, pages 6677–6687, 2021.

A Appendix

A.1 Training details

A.1.1 Model Architecture

As introduced in Section 3, Crossway Diffusion composes of four modules, state encoder, state decoder, action encoder, and action decoder. We follow the same state encoder, action encoder, and action decoder design reported in Diffusion Policy [13]. Each source of the state has its own state decoder for the reconstruction task and these state decoders can be categorized into two types based on the type of the state: visual state decoder and low-dimensional state decoder.

The architecture of the visual state decoder is shown in Figure 8. The numbers in the blocks indicate the number of output channels except for ConvTranspose. ConvTranspose doubles the spatial resolution of the input tensor while keeping the number of channels identical.

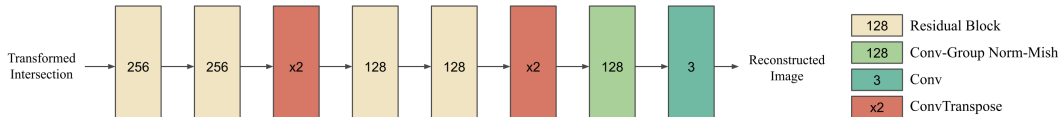


Figure 8: Architecture of state decoder for image reconstruction.

The low-dimensional state decoder is a three-layer MLP. The widths of the hidden layers are in the ratios of 4:2:1 compared to the width of the low-dimensional states.

A.1.2 Hyperparameters

We align most of the hyperparameters with Diffusion Policy [13]. The observation horizon, action horizon, and action prediction horizon are set to 2, 8, and 16 respectively. The learning rate and weight decay are set to $1e-4$ and $1e-6$ respectively. For both training and inference, we employ 100 diffusion iterations. Detailed hyperparameters regarding image reconstruction and the numbers of learnable parameters are reported in Table 5.

Table 5: Hyperparameters and the number of learnable parameters. ImgRes: the resolution of visual states (Camera views \times W \times H); CropRes: the image resolution after random crop; RecRes: the resolution of reconstruction target; #D-Params: number of parameters in diffusion network; #VE-Params: number of parameters in state encoder; #VD-Params: number of parameters in state decoder.

Task	ImgRes	CropRes	RecRes	#D-Params	#VE-Params	#VD-Params
Square	$2 \times 84 \times 84$	$2 \times 76 \times 76$	$4 \times 84 \times 84$	256M	22M	6M
Transport	$4 \times 84 \times 84$	$4 \times 76 \times 76$	$4 \times 60 \times 60$	264M	45M	12M
Tool Hang	$2 \times 240 \times 240$	$2 \times 216 \times 216$	$2 \times 80 \times 80$	256M	22M	6M
Push-T	$1 \times 96 \times 96$	$1 \times 84 \times 84$	$1 \times 96 \times 96$	252M	11M	2M
Duck Lift	$2 \times 160 \times 120$	$2 \times 144 \times 108$	$2 \times 80 \times 60$	255M	22M	6M

A.2 More Reconstruction examples

In Figure 10, we provide additional examples of image reconstruction by visual state decoder of Crossway Diffusion.

A.3 Code and dataset

The code and the real-world dataset Duck Lift will be publicly available soon.

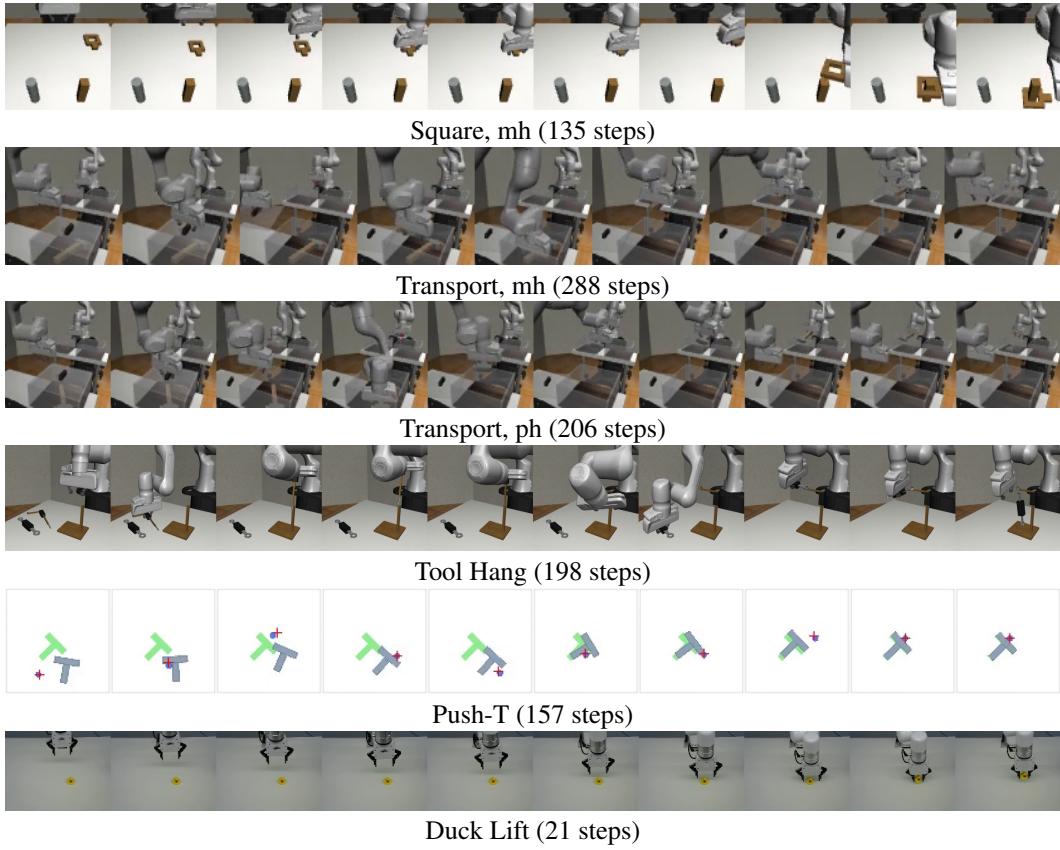


Figure 9: Example episodes of Crossway Diffusion in simulated and real environments. The episode length is reported as well.

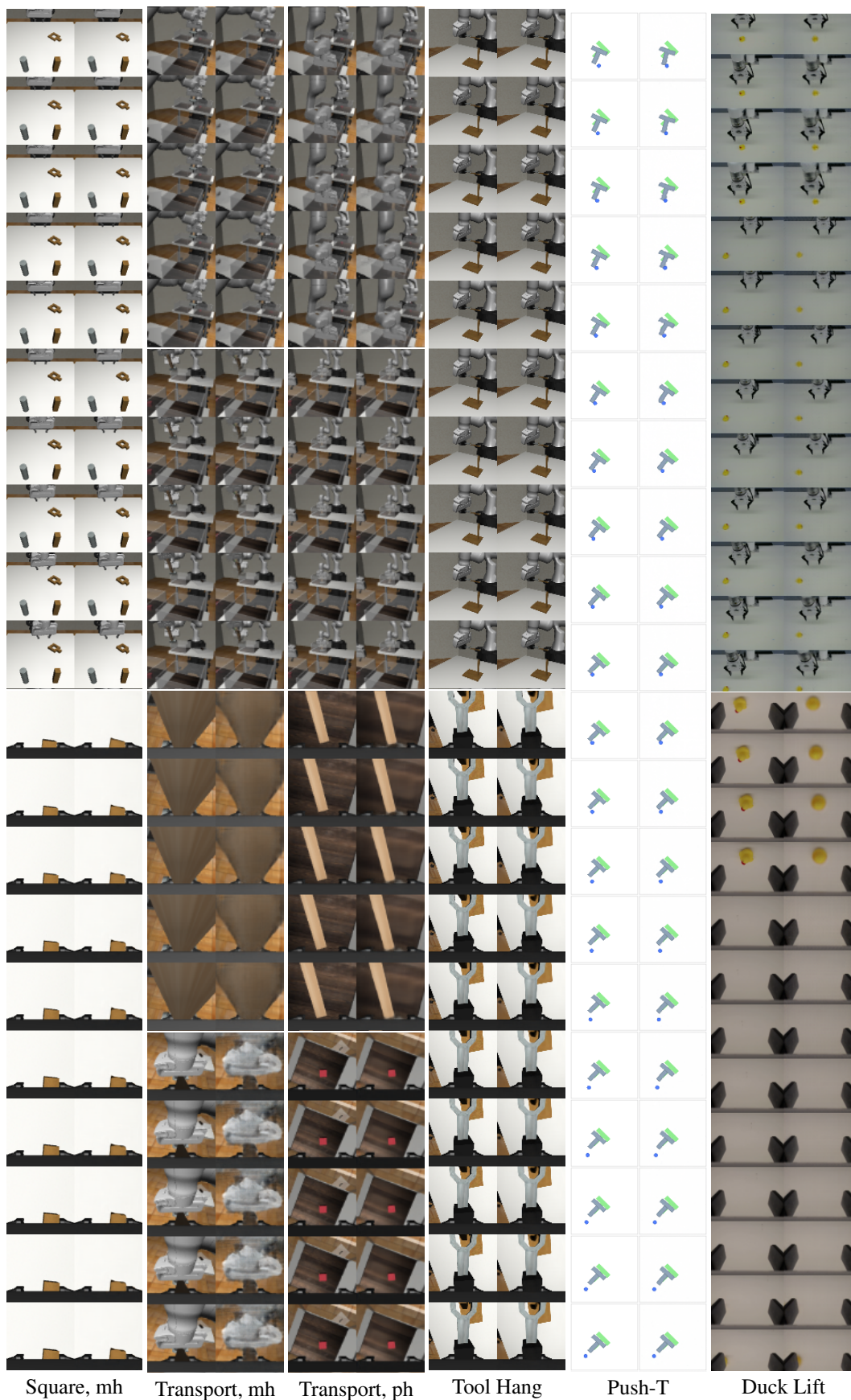


Figure 10: More reconstruction results on the validation set. For each dataset, left: original image, right: reconstructed image.